Supporting Information

Neftci et al. 10.1073/pnas.1212083110

SI Text

Dynamics of the Neural Soft State Machines. We observed that the performance of the system can critically depend on the input duration. This is especially true in the case of ambiguous situations occurring when one input can induce a transition from both the current and the next state. If an input signal is too long, multiple transitions may occur; if it is too short, it may not be able to initiate a transition at all. The steady-state analysis of the system cannot account for this effect. To counter this problem and derive an adequate input duration, we consider the temporal dynamics of the system.

Assuming that only two state populations are active during a transition and all others are silent, we can reduce the system to $N=2$ states S_1 and S_2 with transitions $S_1 \xrightarrow{a} S_2$ and $S_2 \xrightarrow{a} S_1$. We show that as long as the input a is applied, the activity oscillates between these two states. Half the period of this oscillation constitutes an adequate input duration. In the linear threshold unit (LTU) approximation, the dynamics of the two-state system are described by the set of equations

$$\begin{aligned}
\tau_E \dot{x}_1 &= -x_1 + \sigma(w_E x_1 - w_{IE} x_I + \phi_1 z_2 - T_E),\\
\tau_E \dot{x}_2 &= -x_2 + \sigma(w_E x_2 - w_{IE} x_I + \phi_1 z_1 - T_E),\\
\tau_I \dot{x}_I &= -x_I + \sigma(w_{EI}(x_1 + x_2) - T_I),\\
\tau_E \dot{z}_1 &= -z_1 + \sigma(w_{ET} z_1 - w_{IE} z_I + \phi_2 x_1 - T_E + b_{in}),\\
\tau_E \dot{z}_2 &= -z_2 + \sigma(w_{ET} z_2 - w_{IE} z_I + \phi_2 x_2 - T_E + b_{in}),\\
\tau_I \dot{z}_I &= -z_I + \sigma(w_{EI}(z_1 + z_2) - T_I),
\end{aligned}$$

where $x_{1,2}$ and $z_{1,2}$ are the state and transition populations, respectively, x_I and z_I are the inhibiting populations of the respective sWTAs, and $w_E = \alpha + \gamma$.

Assuming that all units are active at any time, we can identify the nonlinearity σ with the identity function. Using the substitutions $x_+ = x_1 + x_2$, $x_- = x_1 - x_2$, $z_+ = z_1 + z_2$, and $z_- = z_1 - z_2$, we can decouple the equations and obtain two independent systems,

$$\begin{aligned}
\tau_E \dot{x}_+ &= -x_+ + w_E x_+ - 2 w_{IE} x_I + \phi_1 z_+ - 2T_E,\\
\tau_E \dot{z}_+ &= -z_+ + w_{ET} z_+ - 2 w_{IE} z_I + \phi_2 x_+ - 2T_E + 2b_{in},\\
\tau_I \dot{x}_I &= -x_I + w_{EI} x_+ - T_I,\\
\tau_I \dot{z}_I &= -z_I + w_{EI} z_+ - T_I,
\end{aligned}$$

and

$$\begin{aligned}
\tau_E \dot{x}_- &= -x_- + w_E x_- - \phi_1 z_-,\\
\tau_E \dot{z}_- &= -z_- + w_{ET} z_- + \phi_2 x_-.
\end{aligned}$$

For the parameters from Table S1 and $\tau_i < \tau_e$ the first system has a stable fixed point $\lim_{t\to\infty}(x_+, z_+, x_I, z_I) = (x_+^\infty, z_+^\infty, x_I^\infty, z_I^\infty)$. Thus, for $t \gg 0$, the dynamics are governed by the second system, which has an unstable fixed point at $(0,0)$. The system can be solved and, for the parameters from Table S1, yields a solution

$$x_-(t) = x_0 e^{\frac{w_E + w_{ET}}{2\tau_e} t} \sin\left(\frac{\sqrt{4\phi_1\phi_2 - (w_E - w_{ET})^2}}{2\tau_e} t + \rho \right),$$

where x_0 and ρ are constants.

The oscillating part of the solution reflects the oscillation of the system between the two states S_1 and S_2 and leads to a transition duration, i.e., the time taken by the state-holding population to rise from zero to peak activity, of

$$t_{trans} = \frac{2\pi\tau_e}{\sqrt{4\phi_1\phi_2 - (w_E - w_{ET})^2}}.$$

The cyclic two-state soft state machine (SSM) described here has been simulated both spike based and as a system of LTUs with the parameters displayed in Table S1. The spiking system contained 150 neurons per population and the connection probabilities were multiplied by a factor of 16/150 to reflect the overall connection strength used in our hardware experiments. The larger number of neurons reduced the activity fluctuations and allowed a clearer readout of the transition frequency. As shown in Fig. S2, the analytic result is in good agreement with the simulations. For the parameters from Table S1 and a time constant $\tau_E = 50$ ms the estimated transition duration equals $t_{trans} = 305$ ms, which is in the scope of the value used in our experiments.

Nullcline Analysis for the Calculation of b_{min}. Here, we explicitly compute the input $b_{\min}$ necessary to perform a transition from state pre to state post. The equations describing the dynamics of pre and post are

$$\begin{aligned}
\tau_E \dot{x}_{\text{pre}} + x_{\text{pre}} &= \sigma\left(w_E x_{\text{pre}} - w_{IE} w_{EI}\left(x_{\text{pre}} + x_{\text{post}}\right) + c\right),\\
\tau_E \dot{x}_{\text{post}} + x_{\text{post}} &= \sigma\left(w_E x_{\text{post}} - w_{IE} w_{EI}\left(x_{\text{pre}} + x_{\text{post}}\right) + c + b\right).
\end{aligned}$$

To calculate $b_{\min}$, we study the stability of the fixed points in this system, using a phase plane analysis. The nullclines of this system are the curves defined by $\dot{x}_{\text{post}} = 0$ and $\dot{x}_{\text{pre}} = 0$:

$$\left\{ \left(x_{\text{post}}, x_{\text{pre}}\right) \middle| \; x_{\text{post}} = \begin{cases} \dfrac{-w_{EI} w_{IE} x_{\text{pre}} + c + b}{\Lambda}, & \text{if } \; x_{\text{pre}} < \dfrac{c+b}{w_{EI} w_{IE}}; \\ 0, & \text{otherwise;} \end{cases} \right\}$$

$$\left\{ \left(x_{\text{post}}, x_{\text{pre}}\right) \middle| \; x_{\text{pre}} = \begin{cases} \dfrac{-w_{EI} w_{IE} x_{\text{post}} + c}{\Lambda}, & \text{if } \; x_{\text{post}} < \dfrac{c}{w_{EI} w_{IE}}; \\ 0, & \text{otherwise.} \end{cases} \right\}.$$

These curves are illustrated in Fig. S4, where $c = (w_{IE} T_I - T_E)$. The arrows in Fig. S4 indicate the direction of the gradient at both sides of the nullclines. By definition of the nullcline, the direction of the gradient vector does not change within either side of the nullcline. This analysis provides a visual and intuitive indication on the stability associated with the fixed points (situated at the crossings of the nullclines). If both vectors point toward the fixed point, then it is stable. In any other case the fixed point is unstable. We observe that the fixed points on the axes are stable, whereas the fixed point in the middle is unstable.

The effect of an input $b > 0$ to post is to shift the linear portion of the nullcline toward the right. According to Fig. S4, when the input reaches a critical magnitude, the central fixed point (which is unstable) merges with the fixed point associated with pre being active, which then loses stability. The only stable fixed point of the system becomes the one associated with post. A simple calculation shows that an input $b_{\min} = c\left(\frac{w_{IE} w_{EI}}{\Lambda} - 1\right)$ suffices.

List of Parameters. The parameters displayed below were measured once the parameter calibration procedure described in ref. 1 was completed. The measurements of the synaptic efficacies were carried out as explained in ref. 1. The inhibitory couplings were the same for both transitions soft winner-take-all (sWTA) and state-holding sWTA. Our choice of parameters is not optimal with respect to stability and performance because of hardware constraints, namely in the number of available synapses and leak currents. Because the leak is a global parameter, state-holding units and transition units were forced to share T_E. Due to constraints in the number of independent synapse parameters, the connection probabilities ranged from 20% to 100%. However, the neural model allows much smaller probabilities [e.g., around 10% (2)] and this could be easily achieved in hardware as well by introducing a larger number of independent synapse parameters.

1. Neftci E, Chicca E, Indiveri G, Douglas R (2011) A systematic method for configuring VLSI networks of spiking neurons. *Neural Comput* 23(10):2457–2497.
2. Brunel N (2000) Dynamics of sparsely connected networks of excitatory and inhibitory spiking neurons. *J Comput Neurosci* 8(3):183–208.

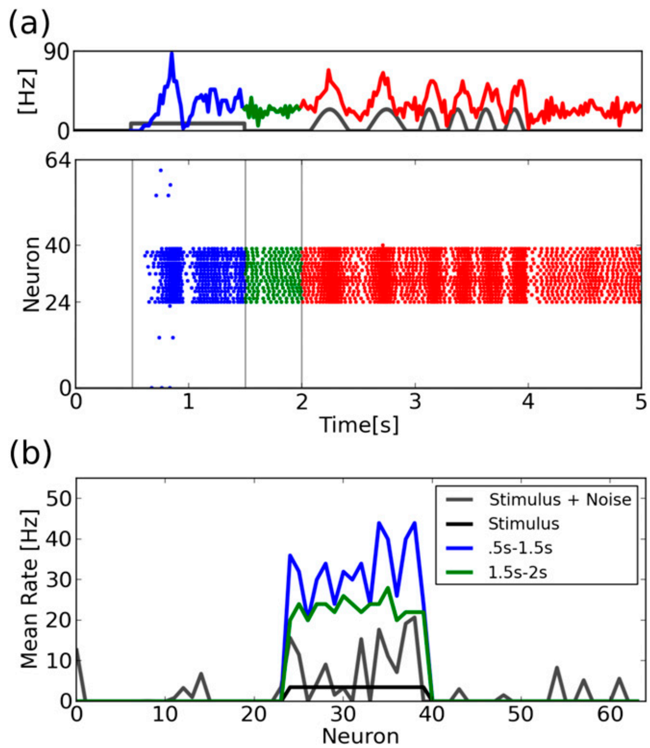

Fig. S1. Signal restoration in the sWTA and coexistence of digital selection and analog amplification. We simulate a network of integrate-and-fire (I&F) neurons to demonstrate the signal restoration property of the sWTA, using the same parameters as in the state-holding sWTA populations (Table S1). In addition to the sWTA couplings, there are recurrent connections between neurons 24 and 40. (*A*) Raster plot of a trial run (*Lower*) and firing rate of neurons 24–40 (*Upper*). The sWTA is stimulated by a box-shaped signal corrupted by noise, from 0 s to 1.5 s (black). (*B*) Mean firing rates of the stimulus and network activity. After an initial transient, the feedback in the network amplifies the signal and restores it toward the stored pattern (blue, 0.5–1.5 s). The resulting activity still reflects the stimulus profile, but after the stimulus is removed, the activity persists and is shaped only by the pattern stored in the couplings (green, 1.5–2 s). The circuit thus interprets an incomplete or noisy input signal by restoring it toward the pattern embedded in its connections. During times 2–4 s, all of the excitatory neurons are stimulated by an oscillatory signal (red, 2–3 s, 2 Hz; 3–4 s, 4 Hz), and the activity in the sWTA reflects this analog signal in the active attractor state only (neurons 24–40; the other neurons are inhibited). This illustrates the coexistence of digital selection (the active pattern) and the analog signal amplification properties of the sWTA (1). The memory is analog in the sense that the attractor can modulate its activity to reflect spatial and temporal changes in its inputs. These are well-known properties of attractor networks; see, e.g., ref. 2. In the plots, the firing rates of the stimuli were multiplied by the input synapse weight (0.015) and subtracted by T_{exc} to emphasize the effect of the recurrent connections. In addition to the parameters in Table S1, we used $\tau_{exc} = 80$ ms, $\tau_{inh} = 50$ ms.

1. Hahnloser R, Sarpeshkar R, Mahowald MA, Douglas RJ, Seung S (2000) Digital selection and analog amplification co-exist in an electronic circuit inspired by neocortex. *Nature* 405(6789):947–951.
2. Amit DJ, Brunel N (1997) Dynamics of a recurrent network of spiking neurons before and following learning. *Network* 8(4):373–404.

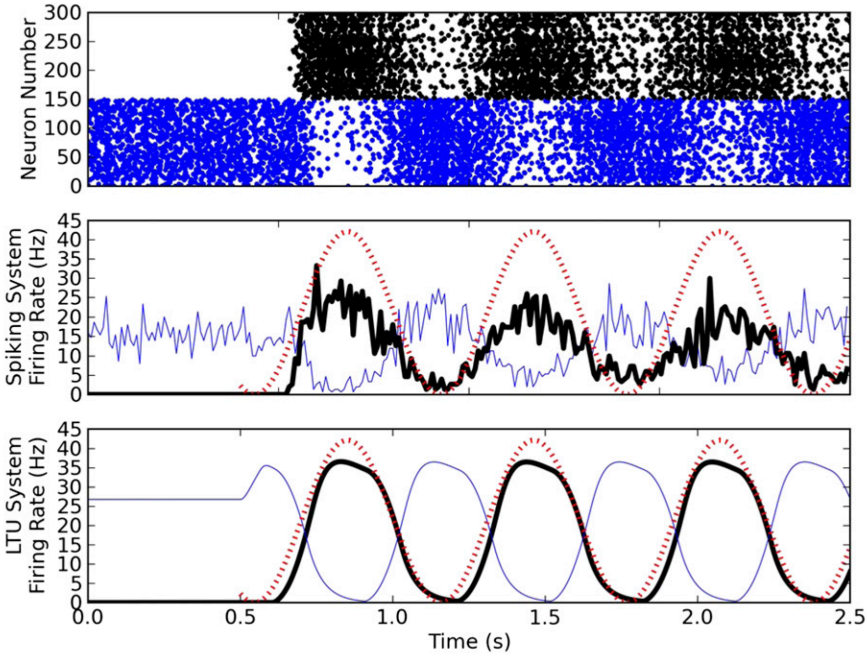

Fig. S2. Oscillations in the cyclic SSM configuration. The cyclic two-state SSM has been simulated both spike based (as a system of I&F neurons) and as a system of LTUs. Shown are the spiking activity of the two state populations (*Top*), the mean firing rates of the same populations (*Middle*; bin size 10 ms), and the rates in the LTU approximation (*Bottom*). The activity of the two state populations is plotted in black and blue. The oscillating part of the analytic solution is shown as a red, dotted line.

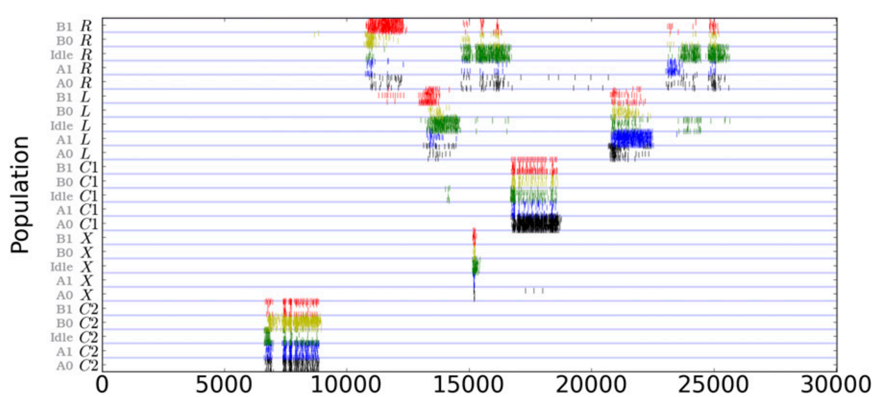

Fig. S3. Activity of the transition sWTA in the pattern recognition task. This raster plot presents the spiking activity of the transition populations in the trial presented in Fig. 4. Each population represents one possible transition (an arrow in the state diagram, Fig. S1). The selective attention chip (SAC) stimulates a group of transition populations receptive to the location of the active neuron. The population previously stimulated by an active state wins the competition and drives the transition to a new state. The spatial variability observed in the spiking responses is mostly due to fabrication mismatch.

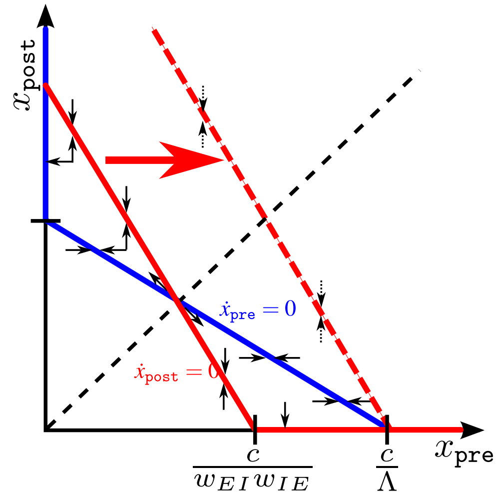

Fig. S4. Phase plane analysis of state transition and calculation of $b_{\min}$. The nonlinear system has three fixed points that are situated at the crossings of the two nullclines (red and blue). The black arrows indicate the direction of the gradient at both sides of the nullclines. The central fixed point is always unstable but the two other fixed points situated on the axes can be stable. Applying an input to post shifts its nullcline to the right (red dashed line). The analysis illustrates that, if the input b is larger than $\frac{b_{min}}{\Lambda}$, the fixed point situated on the horizontal axis $(x_{\mathrm{pre}} = \frac{c}{\Lambda})$ loses stability. This provides us with the minimum input required to induce transition from pre to post.

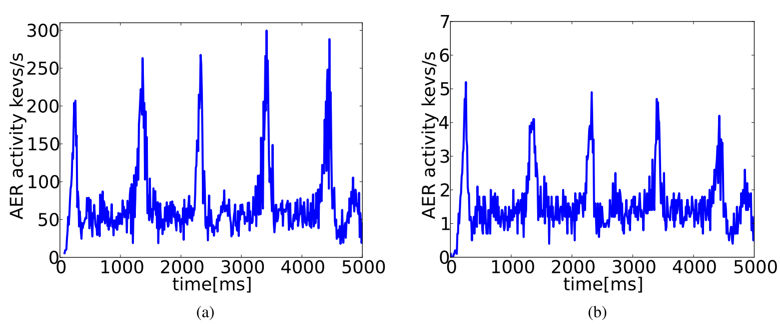

Fig. S5. Total monitored and mapped address-event representation (AER) activity in an example SSM. We measure the AER communication in a randomly generated SSM of dimensions $N_s = 5$, $N_q = 5$, without ambiguous transitions. (*A*) Number of mapped (routed) address events per second, corresponding to the AER traffic. The positions of the peaks correspond to the times when the inputs were provided. (*B*) Number of monitored address events, corresponding to neurons that have spiked.

Table S1. Parameters used for the soft state machine

Parameter	Value	Description
α	0.94	Weight of recurrent excitative couplings within state-holding sWTA
w_{ET}	0.74	Weight of recurrent excitative couplings in transition sWTA
w_{EI}	0.47	Weight of excitative couplings from excitatory to inhibitory neurons
w_{IE}	6.06	Weight of inhibitive couplings from inhibitory to excitatory neurons
γ	0.68	Weight of recurrent excitative couplings between state-holding sWTAs
$\phi 1$	0.21	Weight of excitative coupling from old state to transition populations
$\phi 2$	2.18	Weight of excitative coupling from transition population to new state
p_{α}	0.7	Connection probability of α couplings
p_{ET}	0.55	Connection probability of w_{ET} couplings
p_{EI}	0.5	Connection probability of w_{EI} couplings
p_{IE}	0.5	Connection probability of w_{IE} couplings
p_{γ}	0.8	Connection probability of γ couplings
p_{ϕ_1}	0.25	Connection probability of ϕ_1 couplings
p_{ϕ_2}	1.0	Connection probability of ϕ_2 couplings
T_E	7 Hz	Excitatory neuron threshold
T_I	11 Hz	Inhibitory neuron threshold
b_{in}	15.94 Hz	Firing rate of external input to transition population, weighted by input synapse
$b_{\min}$	29.21 Hz	Minimum firing rate of input to state population needed to initiate transition